Life-Cycle of Structures and Infrastructure Systems – Biondini & Frangopol (Eds)

Indirect bridge damage detection using frequencies identified from vibrations of a single two-axle vehicle

Z. Li, W. Lin & Y. Zhang
Department of Civil Engineering, Aalto University, Espoo, Finland

ABSTRACT: Bridge frequency identification using passing vehicles has been demonstrated as a promising approach in the last two decades. Compared to the traditional method that requires sensor systems installed on the bridge, the indirect method only needs a few sensors mounted on passing vehicles, making it potential to monitor a large number of bridges rapidly and economically. However, currently, most studies just checked the existence of the bridge's frequencies in the vehicle's vibrations and explored to identify its frequencies accurately. Few studies investigated the damage detection of bridges using indirectly extracted bridge frequencies. This paper presents an indirect bridge damage detection method using bridge frequencies identified from a passing two-axle vehicle's vibration data. Initially, the bridge's finite element model is carefully built, updated, and divided into several substructures. Damage factors of different substructures are utilized to represent their damage degrees. Then, the bridge's frequencies will be identified from the passing vehicle's vibrations. At this stage, contact-point responses of the vehicle are back-calculated from its accelerations, and the residual contact-point responses of the two axles are employed to eliminate the vehicle's frequencies and inverse effects of road roughness, making the bridge's frequencies highlighted in the frequency domain. Thirdly, an objective function based on numerical experiments is proposed to locate and quantify the damage. The proposed method is verified numerically by a half-car model and a simply supported bridge in this paper. The results indicate that both the locations and degrees of damage can be identified under different influence factors and show great potential in practical applications.

1 INTRODUCTION

The safety of bridge structures has been a concern in the last decades due to their deterioration and collapse (Barker 2022). Structural health monitoring (SHM) can provide essential techniques for bridge health condition assessment (Bao et al. 2019). Mature approaches have been developed by scholars using sensors installed directly on the bridge (the direct method). However, conventional methods typically need a large number of sensors mounted on the target bridge to form a sensing system, which is expensive and time-consuming.

To monitor the bridge indirectly, the drive-by method was proposed by Yang et al. (2004). The idea just requires several sensors adequately installed on the vehicle rather than the bridge (the indirect method), thus is economical and easy-to-operate. Since CP responses have nothing to do with the vehicle, no vehicle frequencies will appear in the frequency-domain spectrum, Yang et al. (2022) proposed to identify the bridge's frequencies using residual CP responses of a half-car model. Employing CP responses of the vehicle can improve the precision of identifying the bridge's frequencies. However, currently, few studies explored locating and quantifying the bridge's damage using the indirectly identified frequencies. The substructure isolation method is one of the effective methods to identify structural damage, in which the substructure is separated from the whole structure and thus can be analyzed individually (Hou et al. 2011, 2019, 2020a; Li et al. 2022). Combined with the indirect method, it has the potential to identify the bridge's damage indirectly.

DOI: 10.1201/9781003323020-43

This paper aims to locate and quantify the bridge's damage using indirectly identified bridge frequencies from the passing vehicle. Firstly, the equations for back-calculating CP responses using the half-car model with four Degrees of freedom (DOFs) are derived. Then, an objective function employing the identified frequencies is proposed. Thirdly, a numerical experiment is carefully designed to verify the proposed method. The remainder of this paper is structured as follows: Section 2 introduces the theoretical foundations for calculating CP responses and building objective functions. Section 3 provides the numerical simulation of a Vehicle Bridge Interaction (VBI) system and discusses several damage cases and influencing factors. Finally, this paper is concluded in Section 4.

2 THEORETICAL FOUNDATIONS

2.1 *CP responses*

2.1.1 *VBI model*

This section employs a half-car model with four DOFs, and the bridge is simulated by a simply supported beam, as illustrated in Figure 1. The finite element (FE) model for the VBI system is built in MATLAB.

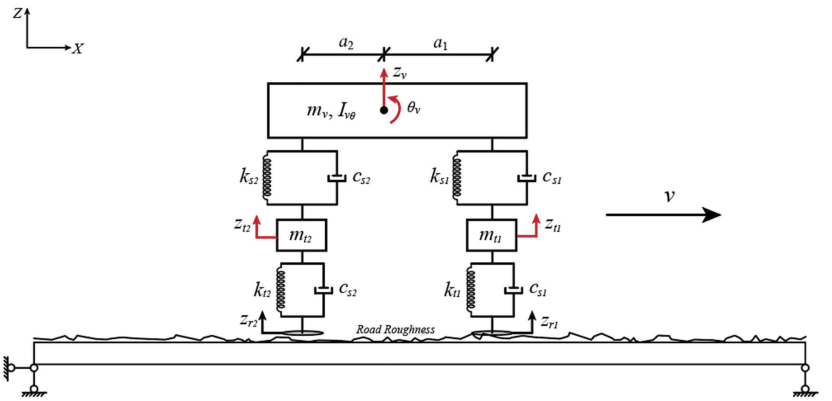

Figure 1. Half-car model and the simply supported beam.

In Figure 1, four DOFs of the vehicle are illustrated by red arrows. They are vehicle body bounce z_v, body pitching θ_v, and bounces of front and rear axles z_{t1}, z_{t2}. The displacements between the tire and road profile are represented by u_{c1} and u_{c2}. The mass of the vehicle body is m_v, and its pitching moment of inertia is $I_{v\theta}$. The masses for front and rear axles (including wheels) are m_{t1} and m_{t2}, respectively. The distances between the gravity center and front and rear axles are a_1 and a_2. The stiffness and damping of the suspension system are represented by k_{s1}, k_{s2}, c_{s2}, c_{s2}, and for the tires, they are k_{t1}, k_{t2}, c_{t2}, c_{t2} respectively. The vehicle's speed is denoted by v. The vehicle's dynamic equilibrium equation is represented by Equation (1),

$$\mathrm{M}_v\ddot{\mathbf{z}}(t) + \mathrm{C}_v\dot{\mathbf{z}}(t) + \mathrm{K}_v\mathbf{z}(t) = \boldsymbol{p}_v \tag{1}$$

where M_v, C_v and K_v are the vehicle's mass, damping, and stiffness matrices; $\ddot{\mathbf{z}}(t), \underline{\mathbf{z}}(t)$ and $\mathbf{z}(t)$ are its acceleration, velocity, and displacement vectors, respectively; $\boldsymbol{p}_v$ is the input excitation vector for the vehicle. These matrices are shown in Equations (2~5),

$$\mathrm{M}_v = \begin{bmatrix} m_v & 0 & 0 & 0 \\ 0 & I_{v\theta} & 0 & 0 \\ 0 & 0 & m_{t1} & 0 \\ 0 & 0 & 0 & m_{t2} \end{bmatrix} \tag{2}$$

$$\mathrm{C}_v = \begin{bmatrix} c_{s1}+c_{s2} & a_1c_{s1}-a_2c_{s2} & -c_{s1} & -c_{s2} \\ a_1c_{s1}-a_2c_{s2} & a_1^2c_{s1}+a_2^2c_{s2} & -a_1c_{s1} & a_2c_{s2} \\ -c_{s1} & -a_1c_{s1} & c_{s1}+c_{t1} & 0 \\ -c_{s2} & a_2c_{s2} & 0 & c_{s2}+c_{t2} \end{bmatrix} \tag{3}$$

$$\mathrm{K}_v = \begin{bmatrix} k_{s1}+k_{s2} & a_1k_{s1}-a_2k_{s2} & -k_{s1} & -k_{s2} \\ a_1k_{s1}-a_2k_{s2} & a_1^2k_{s1}+a_2^2k_{s2} & -a_1k_{s1} & a_2k_{s2} \\ -k_{s1} & -a_1k_{s1} & k_{s1}+k_{t1} & 0 \\ -k_{s2} & a_2k_{s2} & 0 & k_{s2}+k_{t2} \end{bmatrix} \tag{4}$$

$$\boldsymbol{p}_v = \begin{bmatrix} 0 \\ 0 \\ k_{t1}u_{c1}+c_{t1}\dot{u}_{c1} \\ k_{t2}u_{c2}+c_{t2}\dot{u}_{c2} \end{bmatrix},\ \boldsymbol{z} = \begin{bmatrix} z_v \\ \theta_v \\ z_{t1} \\ z_{t2} \end{bmatrix} \tag{5}$$

where $u_{ci} = u_{bi} + z_{ri}$, $\dot{u}_{ci} = \dot{u}_{bi} + \dot{z}_{ri}$, and $u_{bi}, \dot{u}_{bi}$ are the bridge's deflection and velocity at the i-th contact point.

For the bridge, it is simply supported at each end, as shown in Figure 1. The beam can be divided into N_b Euler-Bernoulli elements and N_s substructures for damage locating purposes. Each node has two DOFs: vertical transition and rotation. The bridge's vibration equations can be denoted by Equation (6),

$$\mathrm{M}_b\ddot{\mathbf{z}}_b(t) + \mathrm{C}_b\dot{\mathbf{z}}_b(t) + \mathrm{K}_b\mathbf{z}_b(t) = \boldsymbol{p}_b^N \tag{6}$$

where M_b, C_b and K_b are the bridge's mass, damping, and stiffness matrices. In this paper, the damping is simulated by the Rayleigh damping assumption, which can be obtained by $\mathrm{C}_b = \alpha\mathrm{M}_b + \beta\mathrm{K}_b$, where α and β can be obtained when the first two order damping ratios ξ_1, ξ_2 are set beforehand.

The interaction of the vehicle and the bridge is accomplished by the tires. When the tires of the vehicle are not on the bridge's nodes, the Hermitian cubic interpolation function is employed to distribute the CP force to its two adjacent nodes. This process can be finished by Equations (7~10),

$$\boldsymbol{p}_b^N = \mathrm{N}_c\boldsymbol{p}_{\boldsymbol{b}} \tag{7}$$

$$\mathbf{p_b} = \begin{bmatrix} k_{t1}(z_{t1}-u_{c1}) + c_{t1}(\dot{z}_{t1}-\dot{u}_{c1}) - m_vg\cdot\frac{a_2}{a_1+a_2} - m_{t1}g \\ k_{t2}(z_{t2}-u_{c2}) + c_{t2}(\dot{z}_{t2}-\dot{u}_{c2}) - m_vg\cdot\frac{a_1}{a_1+a_2} - m_{t2}g \end{bmatrix} \tag{8}$$

$$\mathrm{N}_c = \begin{bmatrix} 0 & \cdots & 0 & \cdots & \boldsymbol{\varphi}_1 & \cdots & 0 \\ 0 & \cdots & \boldsymbol{\varphi}_2 & \cdots & 0 & \cdots & 0 \end{bmatrix}^T \tag{9}$$

$$\boldsymbol{\varphi}_i = \begin{bmatrix} 1-3d_i^2+2d_i^3 \\ d_il_e(d_i-1)^2 \\ 3d_i^2-2d_i^3 \\ d_il_e(d_i^2-d_i) \end{bmatrix}^T,\ d_i = \frac{x_i(t)-(j-1)l_e}{l_e} \tag{10}$$

where $x_i(t)$, i = 1,2 is the distance of the i-th contact points on the j-th element to the bridge's left end at t time, and l_e is the length of the bridge's element. By employing the Newmark-β method, we can get the bridge's deflections at nodes, namely $\boldsymbol{z}_b$. Then the deflection at contact points can be calculated using $\boldsymbol{u}_b = \mathrm{N}_c^T\mathbf{z}_b$, and the velocity can be obtained as $\dot{\boldsymbol{u}}_b = v(\mathrm{N}_c^{'})^T\ \mathbf{z}_b + \mathrm{N}_c^T\dot{\mathbf{z}}_b$. Therefore, Equation (5) can be updated accordingly. After several iterations, the interaction between the vehicle and the bridge can converge at an acceptable precision.

2.1.2 *Road roughness*

In this paper, the road roughness is generated according to ISO 8608 (Technical Committee ISO/TC 1995). The procedure can be represented by Equations (11) and (12),

$$r(x) = \sum_{i=1}^{N} \sqrt{2G_d(n_i)\Delta n}\cos(2\pi n_i x + \theta_i) \tag{11}$$

$$G_d(n_i) = G_d(n_0)\left(\frac{n_i}{n_0}\right)^{-2} \tag{12}$$

where $r(x)$ is the generated road roughness. θ_i is uniformly distributed between 0 and 2π. Δn is selected as 0.01 cycle/m. n_0 is taken as 0.1 cycle/m, and n_i is set as numbers from 0.01 to 10 m^{-1} with an interval of $0.01m^{-1}$. $G_d(n_0)$ will be determined by the road class used in the simulation.

2.1.3 *CP response calculation*

By disassembling Equation (1), we can get the equilibrium equations related to the wheels as shown in Equations (13) and (14).

$$m_{t1}\ddot{z}_{t1} - c_{s1}\left(\dot{z}_v - \dot{z}_{t1} + a_1\dot{\theta}_v\right) - k_{s1}(z_v - z_{t1} + a_1\theta_v) + c_{t1}(\dot{z}_{t1} - \dot{u}_{c1}) + k_{t1}(z_{t1} - u_{c1}) = 0 \tag{13}$$

$$m_{t2}\ddot{z}_{t2} - c_{s2}\left(\dot{z}_v - \dot{z}_{t2} - a_2\dot{\theta}_v\right) - k_{s2}(z_v - z_{t2} - a_2\theta_v) + c_{t2}(\dot{z}_{t2} - \dot{u}_{c2}) + k_{t2}(z_{t2} - u_{c2}) = 0 \tag{14}$$

By taking the second order derivative of Equations (13) and (14), and rearranging items related to CP responses, we can get

$$\ddot{u}_{ci} + \frac{c_{ti}}{k_{ti}}\frac{d\ddot{u}_{ci}}{dt} = \Psi_i(t), i = 1, 2. \tag{15}$$

$$\Psi_2(t) = \frac{m_{t1}}{k_{t1}}\frac{d^2\ddot{z}_{t1}}{dt^2} - \frac{c_{s1}}{k_{t1}}\left(\frac{d\ddot{z}_v}{dt} - \frac{d\ddot{z}_{t1}}{dt} - a_1\frac{d\ddot{\theta}_v}{dt}\right) - \frac{k_{s1}}{k_{t1}}\left(\ddot{z}_v - \ddot{z}_{t1} - a_1\ddot{\theta}_v\right) + \ddot{z}_{t1} + \frac{c_{t1}}{k_{t1}}\frac{d\ddot{z}_{t1}}{dt} \tag{16}$$

$$\Psi_2(t) = \frac{m_{t2}}{k_{t2}}\frac{d^2\ddot{z}_{t2}}{dt^2} - \frac{c_{s2}}{k_{t2}}\left(\frac{d\ddot{z}_v}{dt} - \frac{d\ddot{z}_{t2}}{dt} - a_2\frac{d\ddot{\theta}_v}{dt}\right) - \frac{k_{s2}}{k_{t2}}\left(\ddot{z}_v - \ddot{z}_{t2} - a_2\ddot{\theta}_v\right) + \ddot{z}_{t2} + \frac{c_{t2}}{k_{t2}}\frac{d\ddot{z}_{t2}}{dt} \tag{17}$$

In Equations (15~17), m_{ti}, c_{ti}, k_{ti} and k_{si} can be measured in experiments. $\ddot{z}_v, \ddot{\theta}_v$ and $\ddot{z}_{ti}$ are collected accelerations when the vehicle is passing the bridge. a_1 and a_2 are constants shown in Figure 1. For first- and second-order derivatives in Equations (16) and (17), they can be calculated by first-order finite difference formulas and second-order central formulas as shown in Equations (18) and (19).

$$\frac{d\ddot{z}_{ti}}{dt} = \frac{\ddot{z}_{ti}(s) - \ddot{z}_{ti}(s-1)}{\Delta t}, \frac{d\ddot{z}_v}{dt} = \frac{\ddot{z}_v(s) - \ddot{z}_v(s-1)}{\Delta t}, \frac{d\ddot{\theta}_v}{dt} = \frac{\ddot{\theta}_v(s) - \ddot{\theta}_v(s-1)}{\Delta t} \tag{18}$$

$$\frac{d^2\ddot{z}_{ti}}{dt^2} = \frac{\ddot{z}_{ti}(s+1) - 2\ddot{z}_{ti}(s) + \ddot{z}_{ti}(s-1)}{(\Delta t)^2} \tag{19}$$

We can see that Equation (15) is a first-order linear differential equation. Its solution can be represented by Equation (20), and due to the discrete data collection, it can be rewritten as Equation (21),

$$\ddot{u}_{ci}(t) = \begin{cases} \Psi_i(t), i = 1, 2. \ if \ c_{ti} = 0 \\ \frac{k_{ti}}{c_{ti}}\exp\left(-\frac{k_{ti}}{c_{ti}}t\right)\left(\int_0^t \psi_i(\tau) exp\left(\frac{k_{ti}}{c_{ti}}\tau\right)d\tau\right), i = 1, 2., if \ c_{ti} \neq 0 \end{cases} \tag{20}$$

$$\ddot{u}_{ci}(t) = \begin{cases} \Psi_i(t), i = 1, 2. if\ c_{ti} = 0 \\ \frac{k_{ti}}{c_{ti}} \left(\sum_{c_{ti}}^{t/\Delta t} \Psi_i|_s \exp\left(\frac{k_{ti}}{c_{ti}} (s\Delta t - t) \right) \Delta t \right), i = 1, 2;\ s = 1, 2 \cdots if\ c_{ti} \neq 0 \end{cases} \tag{21}$$

where Δt is the sampling time interval, and s represents the s-th sampling point of the vehicle's accelerations.

2.2 *Objective function*

After the bridge's frequencies are extracted from the vehicle's vibrations, the next step is to identify the possible damage to the bridge. The proposed method requires a FE model of the undamaged bridge. As introduced in Equation (6), the mass, damping, and stiffness matrices of the undamaged bridge can be represented by $\mathrm{M_b}$, $\mathrm{C_b}$, and $\mathrm{K_b}$. The bridge is divided into N_s substructures, and its damage degree can be denoted by damage factors $\boldsymbol{\mu} = \left[\mu_1,\ \mu_2, \ldots, \mu_{N_s}\right]^T$, in which μ_i represents the damage factor of the i-th substructure. If the damage factor $\mu_i < 1$, it means that the i-th substructure is damaged, and the damage degree is $1 - \mu_i$. If K_{bi} is employed to represent the stiffness matrix of the i-th substructure in the global coordinates, the possibly damaged bridge's stiffness matrix can be calculated by Equation (22),

$$\mathrm{K}_b^d(\boldsymbol{\mu}) = \sum\nolimits_{i=1}^{N_s} \mu_i \mathrm{K}_{bi} \tag{22}$$

where $\mathbf{K}_b^d(\boldsymbol{\mu})$ is the stiffness matrix of the possibly damaged bridge. The objective function using frequencies can be represented by Equation (23),

$$\Delta(\boldsymbol{\mu}) = \sum\nolimits_k^K \left(\frac{\widehat{\omega}_k(\mu) - \omega_k}{\omega_k} \right)^2 + \lambda \|1 - \boldsymbol{\mu}\| \tag{23}$$

where $\hat{\omega}_k(\boldsymbol{\mu})$ is the natural frequencies calculated by the eigenvalue decomposition of $\mathrm{M_b}$ and $\mathrm{K}_b^d(\mu)$. K means the first K order frequencies will be utilized for damage detection. ω_k is the k-th order natural frequency indirectly identified from the passing vehicle. The term $\lambda\|1 - \mu\|$ is the l_1-norm of 1-$\boldsymbol{\mu}$. Such a term is a typical approach that promotes the sparsity of identified damage (Hernandez 2014; Hou et al. 2020b). The damage factors of the damaged bridge can be obtained by optimizing $\boldsymbol{\mu}$ with an initial value.

3 NUMERICAL SIMULATIONS

3.1 *Basic parameters of the VBI system*

The basic parameters of the vehicle and the bridge are listed in Table 1, which is referred to the references (Li et al. 2020; He & Yang 2022).

For the vehicle, its speed is 5 *m/s* when passing the bridge and its frequencies are $f_{v1} \sim f_{v4}$ as shown in Table 1. The axle distance is 4.2 *m*. For the bridge, it is divided into ten substructures and each substructure includes two finite elements as shown in Figure 2. The bridge is simply supported at each end. The bridge's damping is temporarily set as zero and will be discussed in Section 3.3. The sampling frequency is set as 1 kHz.

For the road roughness, an A-class road with $G_d(n0) = 4e^{-6}$ is employed. Due to the tire contact with the road, the original road roughness is smoothed accordingly. The generated road roughness and its PSD are shown in Figures 3 and 4.

3.2 *Bridge frequency identification*

The vehicle's vibrations and responses in the frequency domain are shown in Figure 5. It can be seen from Figure 5 (b) that no bridge's frequencies can be identified using the vehicle's vibrations. The bridge's frequencies have been submerged in the road roughness spectrum and the vehicle's frequency-domain responses. It is hard to identify the bridge's frequency, and further damage detection is unachievable.

Table 1. Basic parameters of the vehicle and bridge.

VBI	Parameters (symbol)	Unit	Value
Vehicle	Body mass (m_v)	kg	17735
	Body moment of inertia $I_{v\theta}$	$kg \cdot m^2$	1.47×10^5
	Axle mass (m_{t1}, m_{t2})	kg	1500,1000
	Suspension damping (c_{s1}, c_{s2})	$N \cdot s/m$	3×10^4, 4×10^4
	Tire damping (c_{t1}, c_{t2})	$N \cdot s/m$	0,0
	Suspension stiffness (k_{s1}, k_{s2})	N/m	2.47×10^6,4.23×10^6
	Tire stiffness (k_{t1}, k_{t2})	N/m	3.74×10^6, 4.6×10^6
	Axle distances (a_1, a_2)	m	2.18,2.02
	Velocity (v)	m/s	5
	Vehicle frequencies (f_{v1}, f_{v2}, f_{v3}, f_{v4})	Hz	1.61,2.29,10.35,15.10
Bridge	Length (l_b)	m	30
	Flexural stiffness (EI)	N/m^2	1.375×10^{10}
	Mass per unit length ($\overline{m}$)	kg/m	2000
	Bridge frequencies (f_{b1}, f_{b2}, f_{b3})	Hz	4.58,18.31,41.19

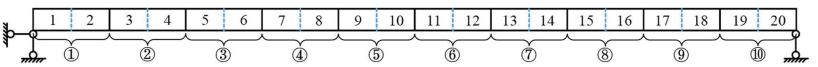

Figure 2. FE model of the bridge.

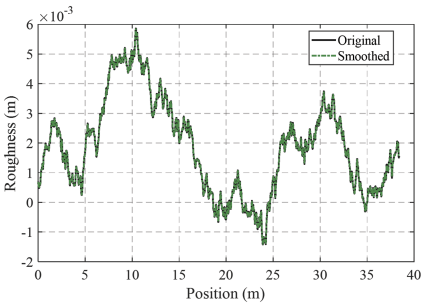

Figure 3. FE model of the bridge.

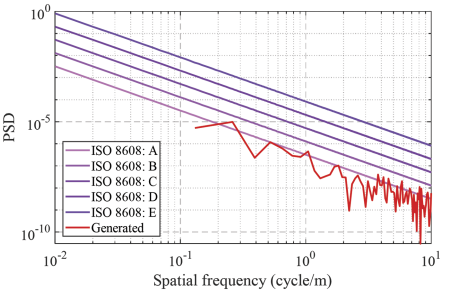

Figure 4. PSD of the road roughness.

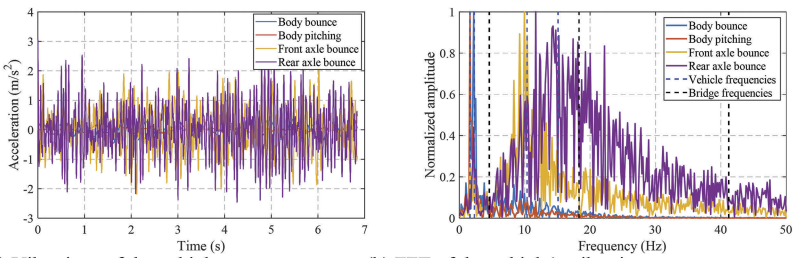

(a) Vibrations of the vehicle (b) FFT of the vehicle's vibrations

Figure 5. Vibrations and FFT spectrum of the vehicle.

To solve the problem, the residual CP responses of the vehicle's two wheels are utilized. After the vehicle's acceleration $\ddot{z}_v, \ddot{\theta}_v, \ddot{z}_{t1}, \ddot{z}_{t2}$ are recorded, CP responses of the front and rear wheels can be back-calculated using Equation (21). Then, to eliminate the inverse effects of road roughness, the residual CP responses of the front and rear tires are utilized. A specific calculation for residual CP responses can be found in reference (Yang et al. 2021). The bridge frequency identification results are shown in Figure 6.

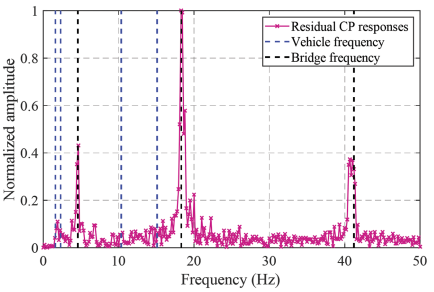

Figure 6. Bridge frequency identification results using residual CP responses.

It can be seen that when the residual CP responses are utilized, the bridge's frequencies are outstanding in the frequency spectrum. Also, for the third frequency, it can be noticed that it has been split into two parts: $f_{b3}^{id1} = f_{b3} - 3\pi v/l_b$ and $f_{b3}^{id2} = f_{b3} + 3\pi v/l_b$. Therefore, in the later damage identification process, the employed bridge's third frequency should be $f_{b3} = (f_{b3}^{id1} + f_{b3}^{id2})/2$.

3.3 *Damage detection*

As discussed in the last sections, it can be seen that when the residual CP responses are employed, the bridge's frequencies can be identified in the frequency domain. However, we can also notice that due to the influence of road roughness, errors in back-calculation of CP responses, and the separation of bridge's frequencies, etc., the accuracy of bridge frequencies cannot be obtained. This section will discuss identifying the bridge's damage using the indirectly identified frequencies. There are two scenarios for the damaged bridge:

(1) Scenario 1: Minor damage, $\boldsymbol{\mu}$ = [1,1,1,1,0.8,1,1,1,1,1].
(2) Scenario 2: Medium damage, $\boldsymbol{\mu}$ = [1,1,0.6,1,1,1,1,1,1,1].

The same FE model used in Section 3.2 is employed for damage detection. Initially, the bridge is assumed as healthy, namely, the initial damage factors are $\boldsymbol{\mu}_0$ = [1,1,1,1,1,1,1,1,1,1]. Then the damage factors are optimized using Equation (23). To verify the applicability of the proposed method, the damage identification results using true frequencies (ω_k^t) of the damaged bridge are also utilized compared with using the indirectly identified frequencies (ω_k) with or without bridge damping. The first three frequencies when the indirect method is employed are utilized for damage detection, namely K=3 in Equation (23).

When the bridge damping is not considered, the bridge's frequencies can be identified well (error $\leq 1.2\%$) as shown in Table 2, and the damage detection results are shown in Figure 7 (red bars). It can be seen from Figure 7 that even though there are some errors between the identified frequencies and the true ones, the bridge's damage can be identified with good precision, especially when the damage degree is low. When the damage degree increases, the damage detection accuracy goes down, and some substructures can be wrongly identified as damaged (e.g., substructure 9 in Figure 7 (b)).

Table 2. Frequencies used for damage detection.

Scenarios	Minor damage scenario			Medium damage scenario		
True frequencies of the damaged bridge ω_k^t/Hz	4.469	18.252	40.464	4.429	17.279	40.083
Identified frequencies without bridge damping $\omega_{k,0}/Hz$ (error)	4.483 (0.31%)	18.276 (0.13%)	40.172 (0.72%)	4.483 (1.2%)	17.414 (0.78%)	40.000 (0.21%)
Identified frequencies with bridge damping $\omega_{k,d}/Hz$ (error)	4.310 (3.56%)	18.621 (2.02%)	40.517 (0.13%)	4.310 (2.69%)	17.069 (1.22%)	40.510 (1.07%)

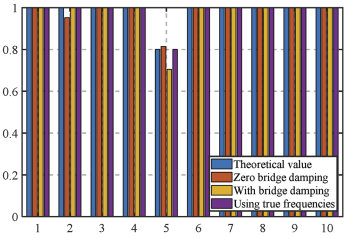

(a) Damage detection results of minor damage

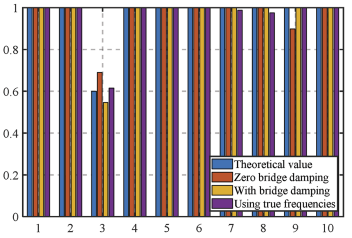

(b) Damage detection results of medium damage

Figure 7. Damage detection results.

When the bridge's damping is assumed as $\xi_1 = \xi_2 = 0.01$. The bridge frequency identification errors increase (error $\leq 3.56\%$) as shown in Table 2. Figure 7 (yellow bars) confirms the effectiveness of the proposed objective function on damage detection. Both the position and degree of the bridge's damage can be detected when the damping is considered. But for the low damage scenario, the identification precision for damage degree decreases compared to the zero-bridge damping results.

4 CONCLUSIONS

In this paper, a damage detection strategy using indirectly identified frequencies of the bridge is proposed. A two-axle half-car model and a simply supported beam are utilized to verify the proposed method. The main concluding remarks are drawn below:

(1) The vehicle's vibrations cannot be directly utilized to identify the bridge's frequencies when the road roughness is considered. By employing residual CP responses, both the vehicle's frequencies and the inverse effects of road roughness can be eliminated, making the bridge's frequencies outstanding and identifiable.
(2) The bridge's damping plays a negative role in identifying the bridge's frequencies. The errors between true and indirectly identified frequencies will increase when the bridge damping is considered.
(3) The proposed damage detection method can be used to locate and quantify the damage even though there are minor errors in indirectly identified bridge frequencies, which shows great potential in engineering applications.

Even though the bridge's damage can be detected with good precision, there are several factors that deserve further studies in engineering, such as multiple damage scenarios, high vehicle speed, engine effects, temperature effects, and ongoing traffics. The investigation of the above factors on damage detection will be included in our future studies before laboratory and field tests.

ACKNOWLEDGEMENTS

This research is fully financially sponsored by the Jane and Aatos Erkko Foundation in Finland (Decision number: 210018). Y. Zhang is financially supported by the Academy of Finland (Decision number: 339493).

REFERENCES

Bao Y., Chen Z., Wei S., Xu Y., Tang Z., & Li H. (2019) The State of the Art of Data Science and Engineering in Structural Health Monitoring. Engineering 5:234–242.

Barker N. (2022) Norway to inspect timber bridges after 10-year-old glulam crossing collapses. https://www.dezeen.com/2022/08/17/norway-timber-tretten-bridge-collapse/. Accessed 24 Aug 2022

He Y. & Yang J.P. (2022) Using acceleration residual spectrum from single two-axle vehicle at contact points to extract bridge frequencies. Eng Struct 266:114538.
Hernandez E.M. (2014) Identification of isolated structural damage from incomplete spectrum information using l1-norm minimization. Mech Syst Signal Process 46:59–69.
Hou J., Jankowski Ł., & Ou J. (2011) A substructure isolation method for local structural health monitoring. Struct Control Heal Monit 18:601–618.
Hou J., Li Z., Jankowski Ł., & Wang S. (2020a) Estimation of virtual masses for structural damage identification. Struct Control Heal Monit 27:1–21.
Hou J., Li Z., Zhang Q., Zhou R., & Jankowski Ł. (2019) Optimal placement of virtual masses for structural damage identification. Sensors (Switzerland) 19:1–18.
Hou J., Li Z., Zhang Q., Jankowski Ł., & Zhang H. (2020b) Local mass addition and data fusion for structural damage identification using approximate models. Int J Struct Stab Dyn 20: 2050124.
Technical Committee ISO/TC (1995) Mechanical Vibration–Road Surface Profiles–Reporting of Measured Data. International Organization for Standardization.
Li J.T., Zhu X.Q., Law S.S., & Samali B. (2020) A Two-Step Drive-By Bridge Damage Detection Using Dual Kalman Filter. Int J Struct Stab Dyn 20: 2042006.
Li Z., Hou J., & Jankowski Ł. (2022) Structural damage identification based on estimated additional virtual masses and Bayesian theory. Struct Multidiscip Optim 65:1–18.
Yang Y.B., Lin C.W., & Yau J.D. (2004) Extracting bridge frequencies from the dynamic response of a passing vehicle. J Sound Vib 272:471–493.
Yang Y.B., Mo X.Q., Shi K., Wang Z.L., Xu H., & Wu Y.T. (2021) Scanning torsional-flexural frequencies of thin-walled box girders with rough surface from vehicles' residual contact response: Theoretical study. Thin-Walled Struct 169:108332.
Yang Y.B., Xu H., Wang Z.L., & Shi K. (2022) Using vehicle–bridge contact spectra and residue to scan bridge's modal properties with vehicle frequencies and road roughness eliminated. Struct Control Heal Monit 29: e2968.